Available online at www.sciencedirect.com

ScienceDirect

Procedia Computer Science 218 (2023) 393–405

Procedia Computer Science

www.elsevier.com/locate/procedia

International Conference on Machine Learning and Data Engineering

Integration of Global and Local Descriptors for Mass Characterization in Mammograms

Devi Vijayan[a], R. Lavanya[b,*]

[a,b]*Department of Electronics and Communication Engineering, Amrita School of Engineering, Coimbatore Amrita Vishwa Vidyapeetham, 641112, India*

Abstract

Breast cancer is the most common cancer among women and is associated with high morbidity and mortality. Early detection has proven successful in effective treatment and increased survival rate. Mammography is the most common modality for screening breast cancer; nevertheless, it is associated with low sensitivity and specificity due to subtlety of abnormalities in early stages. A mass which is the most common and important indicator of breast cancer, is especially challenging to analyse and interpret. Computer aided diagnosis (CAD) systems can improve the diagnostic performance by aiding radiologists in providing an objective assessment. The proposed work aims to develop a CAD system to evaluate mammographic masses and characterize them into benign and malignant categories. The system employs an integrated approach based on fusion of global descriptors extracted from the segmented mass regions and local descriptors from a ribbon of pixels surrounding the mass boundary, to effectively characterize masses. The proposed approach is validated using the Digital Database for Screening Mammograms (DDSM) database, yielding a classification accuracy as high as 94.6% for mass characterization.

Keywords: Computer aided diagnosis; Gray level co-occurrence matrix; Local binary pattern; Masses; Mammography; Scale invariant feature transform.

* Corresponding author. Tel.: +919865816977
E-mail address: r_lavanya@cb.amrita.edu

1877-0509
10.1016/j.procs.2023.01.022

1 Introduction

Globally, cancer is a leading cause of mortality with its incidence projected by World Health Organization (WHO) as 21.6 million in 2030 [1]. Breast cancer is the key contributor of cancer among women. Early diagnosis can significantly reduce the risks associated with breast cancer. Mammography is the most common screening tool for breast cancer, as it depicts very early signs of the disease [2]. However, low contrast of mammograms limits the effectiveness of manual diagnosis, often necessitating follow-up sessions. Computer aided diagnosis (CAD) systems complement radiologists' decisions and could prove to be especially useful in large-scale screening programmes. Radiologists analyse mammograms by assessing visual indicators of breast cancer, among which masses are the most significant. However, benign masses can often be misinterpreted as malignant leading to unnecessary biopsies. This is attributed to the fact that though benign and malignant masses generally exhibit unique characteristics, equivocal cases are not uncommon.

The proposed work aims to develop a CAD system for classifying masses as benign and malignant, using an approach that combines global and local analysis of suspicious regions. The hypothesis underlying this idea is that the heterogeneous nature of these two approaches could pave way for alleviating the ambiguity in characterizing masses. Most of the reported work on mass characterization has been based on global analysis of morphological (shape and margin) and textural characteristics of masses. Verma et al. (2009) extracted density, abnormality rank, shape and margin features from masses. In addition to these global descriptors, age and subtlety factors were also used to build a model based on multilayer perceptron (MLP) and clustering based learning [3]. Liu et al. (2013) extracted geometry and texture features from the candidate mass regions, followed by feature selection for mass characterization using support vector machine (SVM) classifier [4]. Wang et al. (2014) employed Latent Dirichlet Allocation to extract spatial and marginal information from masses. The extracted features were used to train an SVM classifier for mass characterization [5]. Rouhi et al. (2015) extracted intensity, texture and shape features from masses, which was followed by feature selection based on genetic algorithm and classification using neural network [6].

Some researchers focussed on analyzing the region surrounding the mass boundary in contrast to analysing the complete ROI. Statistical and multiresolution analysis of mass boundary and surrounding regions were performed, rather than extracting features that explicitly convey characteristics such as roughness of the boundary. Mudigonda et al. (2000) extracted statistical texture descriptors using gray level co-occurrence matrix (GLCM) applied to a band of pixels, surrounding the mass boundary followed by classification using linear discriminant analysis (LDA) classifier [7]. Midya et al. (2015) analysed the mass region as well as the band of pixels surrounding the mass boundary. Wavelet based multiresolution analysis was performed, followed by determination of angle co-occurrence matrix (ACM) and statistical feature extraction. These features were used as input to a neural network for classification of masses [8].

A few researchers have employed the use of local features for mass characterization. The idea behind this is that local features represent minute details which could not be easily perceived in manual diagnosis. Muramatsu et al. (2016) investigated the use of a segmentation-independent approach involving radial local ternary patterns and neural network classifier [9]. Hua Li et al. (2019) proposed a modified architecture for DenseNet model with Inception structure for mass characterization [10]. Rabidas et al. (2020) extracted a segmentation-independent feature set called local photometric attributes (LPA), followed by step-wise logistic regression for feature selection and LDA for classification [11]. Mohamed W. Abo El-Soud et al. (2020) proposed a scheme involving extraction of orthogonal moment invariant (OMI) features followed by particle swarm optimization (PSO) algorithm for feature selection. The selected features were used to train a SVM classifier for mass characterization [12].

In the proposed work, an integrated approach that combines the merits of global and local analysis has been proposed for classification of masses. The holistic characteristics of masses can be effectively represented using global descriptors, while local descriptors can be utilized for capturing the finer details. In particular, local analysis in the proposed work is performed using a ribbon of pixels surrounding the mass boundary, exploiting the intensity gradient across the margin, which conveys critical information on the mass characteristics. The

remaining sections are structured as follows; Section 2 explains the methodology, followed by result analysis in section 3. Finally, section 4 draws the conclusion.

2. Methodology

The proposed methodology for mammographic mass characterization is illustrated in fig. 2.1. Mammogram images are first subjected to fully automated and optimized region growing based segmentation. Grey wolf optimization (GWO) is employed for determining the optimal seed points and thresholds involved in the region growing process. Global descriptors including morphological features (shape and margin) and gray level co-occurence matrix (GLCM) are employed to effectively represent the comprehensive characteristic of masses. To complement the global analysis, local descriptors including scale invariant feature transform (SIFT) and local binary pattern (LBP), extracted from a ribbon of pixels along the boundary of the mass, are considered. The natural contrast that exists across the boundary between the foreground (masses) and background regions, renders the mass boundary apt for capturing the local variation from the ribbon of pixels surrounding the mass boundary. In this work, an integrated approach that fuses these global and local feature descriptors is proposed for mass characterization, to exploit the complementary nature of the two feature sets.

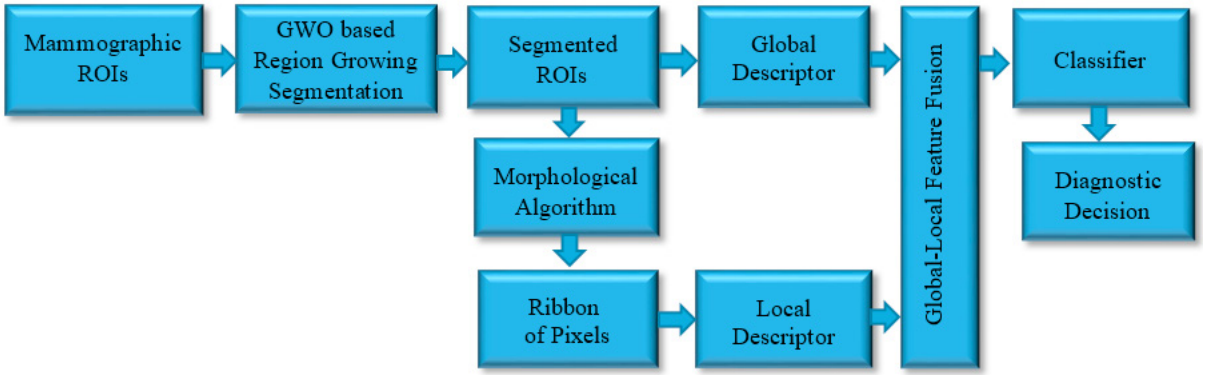

Fig. 2.1 Proposed methodology

2.1 Segmentation

The proposed work employs region growing for segmentation, in which optimal seed points and thresholds are determined using Grey wolf optimization (GWO) [13]. Region growing is an iterative process that typically starts with a single seed point or a set of seed points. The seed pixels are grouped into connected regions based on similarity between pixels. Thresholds are involved in the similarity criteria for grouping of pixels. Employing a global threshold in the region growing process for mammograms leads to inaccurate segmentation due to the high degree of intra and inter-region variability that mammograms exhibit. For the same reason, seed point selection is also not a straight forward process in mammograms.

GWO is a swarm intelligence algorithm motivated by the distinctive behaviour of the grey wolves. It follows the leadership pattern and methods adopted by grey wolves. Grey wolves are categorized into four types, namely, α, β, δ *and* Ω, where α is the highest privileged dominant grey wolf. The characteristic behaviour of grey wolves is hunting, searching, encircling, followed by attacking the prey. The encircling phase is mathematically modelled by equations (1) and (2).

$$\vec{L} = | \vec{N} . \overrightarrow{R_p}(i) - \vec{R}(i) | \tag{1}$$

$$\vec{R}(i+1) = \overrightarrow{R_p}(i) - \overrightarrow{M} . \vec{L} \tag{2}$$

where, $\vec{L}$ is the distance vector of the first three wolves, i denotes the current iteration, $\vec{M}$ and $\vec{N}$ are the coefficient

vectors, $\overrightarrow{Rp}$ is the prey position vector and $\vec{R}$ is the position vector. The vectors $\vec{M}$ and $\vec{N}$ can be obtained using equations (3) and (4).

$$\vec{M} = 2\vec{r}.\ \vec{r}_1 - \vec{r} \tag{3}$$

$$\vec{N} = 2.\ \vec{r}_2 \tag{4}$$

where $\vec{r}$ decreases linearly in the range [2,0] over subsequent iterations and $\vec{r}_1$, $\vec{r}_2$ are random vectors in [0,1].
Based on the three best solutions corresponding to $\alpha, \beta, and\ \delta$ the distance vector and position vector are calculated as in equations (5) and (6), respectively.

$$\vec{L}_\alpha = |\ \vec{N}_1 . \vec{R}_\alpha - \vec{R}\ |;\ \vec{L}_\beta = |\ \vec{N}_2 . \vec{R}_\beta - \vec{R}\ |;\ \vec{L}_\delta = |\ \vec{N}_3 . \vec{R}_\delta - \vec{R}\ | \tag{5}$$

$$\vec{R}_1 = \vec{R}_\alpha\ -\ \vec{M}_1.\ (\vec{L}_\alpha);\ \vec{R}_2 = \vec{R}_\beta\ -\ \vec{M}_2.\ (\vec{L}_\beta);\ \vec{R}_3 = \vec{R}_\delta\ -\ \vec{M}_3.\ (\vec{L}_\delta) \tag{6}$$

Position updation of grey wolves is given by equation (7).

$$\vec{R}(i+1) = \frac{\vec{R}_1 + \vec{R}_2 + \vec{R}_3}{3} \tag{7}$$

The grey wolves stop the hunt once the prey is attacked. Mathematically when $\vec{r}$ decreases to 0, it symbolizes that the movement of prey has stopped. As $\vec{r}$ decreases, $\vec{M}$ also decreases. When $\vec{M}$<1, the wolf is forced to attack the prey, else it diverges from the current position to find a fitter prey. The grey wolf optimization algorithm is summarized in Fig 2.2.

Algorithm for Grey Wolf Optimization

Population initialization $R_j\ (j = 1, 2, .. n)$
Parameter initialization
Fitness function computation, $\vec{R}_\alpha$ *the best search agent, followed by* $\vec{R}_\beta$ *and* $\vec{R}_\delta$
While ($i <$ *maximum iterations)*
  Update the position of search agents
  Perform the parameter updation
  Compute the fitness function
  Update $\vec{R}_\alpha, \vec{R}_\beta$ *and* $\vec{R}_\delta$
  $i = i + 1$
end
return $\vec{R}_\alpha$

Fig. 2.2 Grey wolf optimization algorithm

The optimization of the threshold can be formulated as an objective function using Renyi's entropy method [14], given by equation 8.

$$F_{obj} = Max\ (\sum H_b^a\ (x,y) + \sum H_0^a\ (x,y)) \tag{8}$$

where the term $\sum H_b^a\ (x,y)$ represents entropy of the background region, while $\sum H_0^a\ (x,y)$ represents entropy of the region of interest (ROI). x and y in equation (8) represent the gray-level threshold for a given pixel and average gray level of the neighbouring pixels, respectively.

2.2 Ribbon Extraction

Intensity variations along the mass boundary are relatively higher when compared to the region within the mass.

This is suggestive that local analysis is best performed on a ribbon of pixels along the mass boundary. Fig 2.3 depicts the mass ROI corresponding to a sample mammogram B_0312_1.LEFT_CC.ROI.01 from DDSM dataset, in which the mass boundary, exterior and interior ribbon of pixels are indicated.

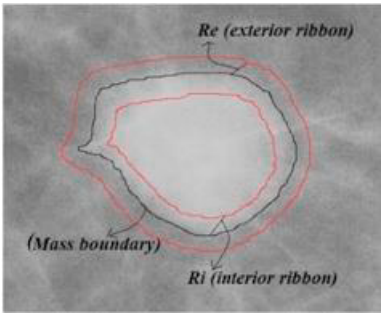

Fig. 2.3 Mammographic ROI: B_0312_1.LEFT_CC.ROI.01 depicting mass boundary with ribbon regions

In the proposed work, morphological operations involving erosion and dilation are performed for ribbon extraction. The exterior ribbon along with boundary is extracted by dilating the segmented binary image $b(x,y)$ using the structuring element $s(x_1,y_1)$, followed by subtracting $b(x,y)$ from dilated image $d(x,y)$. The resultant image is multiplied with the original image $I(x,y)$.

Mathematically, the dilated image $d(x,y)$ is given by equation 9.

$$d(x,y) = b(x,y) \oplus s(x_1,y_1) \tag{9}$$

The binary region $BO(x,y)$ corresponding to the exterior ribbon is given by equation 10.

$$BO(x,y) = d(x,y) - b(x,y) \tag{10}$$

Further, multiplying $BO(x,y)$ with original image $I(x,y)$ yields the gray level counterpart of the ribbon $Re(x,y)$ given by equation 11.

$$Re(x,y) = BO(x,y) \times I(x,y) \tag{11}$$

The dual operation involving morphological erosion is performed to extract the interior ribbon. Initially, the segmented binary image is subjected to erosion, followed by subtracting the eroded image from $b(x,y)$. The resultant image is multiplied with the original image $I(x,y)$.

Mathematically, the eroded image $e(x,y)$ is given by equation 12.

$$e(x,y) = b(x,y) \ominus s(x_1,y_1) \tag{12}$$

The binary counterpart $BI(x,y)$ of the interior ribbon is given by equation 13.

$$BI(x,y) = b(x,y) - e(x,y) \tag{13}$$

Multiplying $BI(x,y)$ with original image $I(x,y)$ represents the gray level counterpart $Ri(x,y)$ of the interior region as shown in equation 14.

$$Ri(x,y) = BI(x,y) \times I(x,y) \tag{14}$$

Finally, the ribbon of pixels is obtained by aggregating the extracted region interior and exterior to the boundary, namely $Ri(x, y)$ and $Re(x, y)$, respectively.

2.3 Feature Extraction

As mentioned earlier, an integrated approach that combines global and local analysis is employed in this work, for mass characterization. This is aimed at leveraging the benefits of both approaches, by effectively capturing the global appearance of the masses which is crucial in determining the mass category as well the local characteristics which capture additional details not restricted to domain knowledge.

2.3.1 Global features

Global features describe ROIs as a whole, necessitating proper segmentation results for effective feature representation. In this work, global features include morphological (shape and margin) and texture features are extracted from segmented masses.

2.3.1.1 Morphological Descriptors

Masses are typically characterized by their morphological properties (shape and margin), that describe their global appearance. As benign and malignant masses typically exhibit variation in these global characteristics, morphological features are considered as important cues for mass characterization. However, proper segmentation of the masses is essential to accurately represent the global appearance of masses using these descriptors. In the present work, a total of 14 morphological descriptors listed in Table 2.1 are extracted [15].

Table 2.1 Morphological descriptors

Sl. No	*Morphological features*	*Description*
1	***Area***	*Total number of mass pixels*
2	***Perimeter***	*Total pixels along mass boundary*
3	***Maximum radius***	*Maximum distance from center of the mass to its edge*
4	***Minimum radius***	*Minimum distance from center of the mass to its edge*
5	***Compactness***	$\left(\frac{2\times\sqrt{Area}\times\pi}{Perimeter}\right)$
6	***Circularity***	$\sqrt{\frac{Area}{\pi\times max\,radius^2}}$
7	***Rectangularity***	$\frac{Area\ of\ ROI}{Area\ of\ the\ minimum\ bounding\ rectangle}$
8	***Aspect ratio***	$\frac{Height\ of\ ROI}{Width\ of\ ROI}$
9	***Elongatedness***	$\left(\frac{Area}{(2\times max\,radius)^2}\right)$
10	***Eccentricity***	$\sqrt{1-\left(\frac{min\,radius}{max\,radius}\right)^2}$
11	***Major axis length***	*Pixel distance between the major-axis endpoints*
12	***Minor axis length***	*Pixel distance between the minor-axis endpoints*
13	***Convexity***	$\frac{O_{convexhull}}{O}$; $O_{convexhull}$ *is the perimeter of convexhull ; O is the perimeter of the original contour*
14	***Euler number***	*Difference between number of connected components and holes*

2.3.1.2 GLCM based-texture features

In this work, texture features are extracted from the segmented masses using gray level co-occurrence matrix (GLCM) [16]. GLCM is used to determine the spatial relationship among pixels and is obtained by computing the probability of paired occurrence of gray level values of an image. In the present work, GLCM is determined by considering the spatial relationship between immediate neighbours in vertical, horizontal and two diagonal directions. A total of 13 statistical features listed in Table 2.2 have been extracted from the GLCM matrix. In the table 2.2, G represents the normalized GLCM matrix; G_{x+y} represents the gray level sum distribution of co-occurring pixels; G_{x-y} represents the gray level difference distribution of co-occurring pixels; n is the total number of gray levels and $\mu_x, \mu_y \; and \; \sigma_x, \sigma_y$ denote the mean and standard deviation along the x and y directions, respectively.

Table 2.2 Statistical measures from GLCM matrix

Sl. No	*Textural Features*	*Mathematical Formula*
1	*Energy(€)*	$€ = \sum_{i=0}^{n-1} \sum_{j=0}^{n-1} G(i,j)^2$
2	*Contrast (C)*	$C = \sum_{i=0}^{n-1} \sum_{j=0}^{n-1} G(i,j)(i-j)^2$
3	*Homogeneity (H)*	$H = \sum_{i=0}^{n-1} \sum_{j=0}^{n-1} \frac{G(i,j)}{(1+(i-j)^2)}$
4	*Variance (V)*	$\sum_{i=0}^{n-1} \sum_{j=0}^{n-1} G(i,j)(i-\mu)^2$
5	*Sum Average (SAVG)*	$SAVG = -\sum_{i=0}^{n-1} iG_{x+y}(i)$
6	*Sum Variance (SVAR)*	$SVAR = -\sum_{i=2}^{2n}(i-SAVG)^2 G_{x+y}(i)$
7	*Sum Entropy (SENT)*	$SENT = -\sum_{i=2}^{2n} G_{x+y}(i)\, lnG_{x+y}(i)$
8	*Difference Entropy (DENT)*	$DENT = -\sum_{i=0}^{n-1} G_{x-y}(i)\, lnG_{x-y}(i)$
9	*Difference Variance (DVAR)*	$DVAR = -\sum_{i=0}^{n-1} G_{x-y}(i)\,(i-DENT)^2$
10	*Information measure of correlation (IC)*	$IC = \frac{ENT+\sum_{i=0}^{n-1}\sum_{j=0}^{n-1} G(i,j)ln(G_x(i),G_y(j)}{\max(-\sum_{i=0}^{n-1} G_x(i)lnG_x(i),-\sum_{j=0}^{n-1} G_y(i)lnG_y(i))}$
11	*Correlation (COR)*	$COR = \frac{\sum_{i=0}^{n-1}\sum_{j=0}^{n-1} G(i,j)(i-\mu_x)(j-\mu_y)}{\sigma_x\sigma_y}$
12	*Entropy (ENT)*	$ENT = -\sum_{i=0}^{n-1}\sum_{j=0}^{n-1} G(i,j)ln(G(i,j))$
13	*Maximum Probability*	$MAXP = MAX_{i,j}\, G(i,j)$

2.3.2 Local features

Local features are useful in capturing the fine details in an ROI so that the subtle textural variation within the ROI can be captured efficiently. In the proposed work, local features that include scale invariant feature transform (SIFT) and local binary pattern (LBP), have been employed.

2.3.2.1 Scale Invariant Feature Transform

Lowe [17] developed the scale invariant feature transform (SIFT), a local feature descriptor for object recognition applications. SIFT descriptors are invariant to rotation, scale and robust to changes in illumination. SIFT key points

are stable extrema points, obtained by using a difference of Gaussian (DoG) function at different scales to identify the maxima and minima. Mathematically, DoG function is given by equation 15.

$$d(x, y, \sigma) = G_F(x, y, k\sigma) - G_F(x, y, \sigma) \tag{15}$$

$$\text{where, } G_F(x, y, \sigma) = G(x, y, \sigma) * M(x, y) \text{ and} \tag{16}$$

$$G(x, y, \sigma) = 1/(2\pi\sigma^2) exp - (x^2 + y^2)/\sigma^2 \tag{17}$$

$G_F(x, y, \sigma)$ is the Gaussian-filtered image, $M(x, y)$ is the input image and $G(x, y, \sigma)$ is the Gaussian function. Each point in the image is compared with its neighbours in the 8-connected neighborhood, and nine neighbours in the next higher and lower scales, to find the extrema points. The extrema are examined and those that exhibit low contrast are eliminated. Based on the gradient, orientation histogram surrounding each key point is computed at a given scale to determine the dominant orientation. The histograms from 4×4 sub regions surrounding each key point are concatenated to form a 128-dimensional feature vector. K-means clustering is applied on the SIFT features of a given image to obtain bag of words (BoW) representation of that image [18].

2.3.2.2 Local Binary Pattern

Local Binary Pattern (LBP) is a texture descriptor obtained by thresholding the neighborhood of each pixel and mapping it to a binary number [19]. If the center pixel is lower than the neighboring value, the corresponding pixel location is assigned as 1, else 0. LBP code extraction is illustrated in Fig. 2.4.

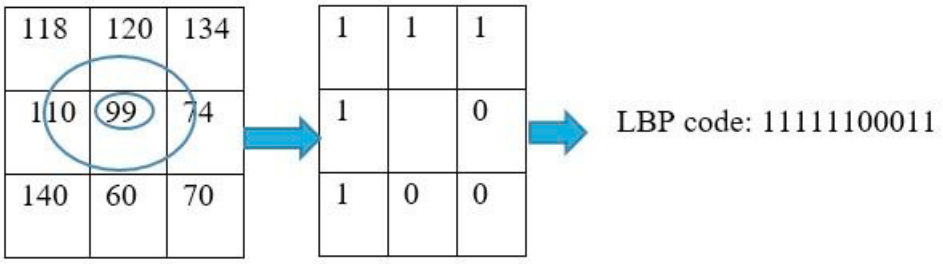

Fig. 2.4 Extraction of local binary pattern

Equation (18) represents the mathematical expression for conventional LBP.

$$LBP_{N,R} = \sum_{n=0}^{N-1} p(i_n - i_c)\, 2^n \tag{18}$$

where $p(.)$ represents the thresholding function given in equation (19).

$$p(t) = \begin{cases} 1, t \geq 0 \\ 0, t < 0 \end{cases} \tag{19}$$

In equation (18), i_c represents the center pixel intensity, i_n represents the n^{th} neighborhood pixel intensity, N denotes the neighborhood pixel count and R denotes the neighborhood radius. In this work, N and R are chosen to be 8 and 1, such that all eight pixels in the neighborhood with a radius 1, are considered. Following the labelling, LBP is finally aggregated to a 256 dimensional feature vector. Uniform LBP, an extension of its conventional counterpart, considers the pattern that contains at most two 0-1 or 1-0 transitions and hence represented by reduced feature dimension of vector length 59. Mathematically, uniform LBP is given in equation (20).

$$LBP_{N,R} = |p(i_{N-1} - i_c) - p(i_o - i_c)| + \sum_{n=0}^{N-1} |p(i_n - i_c) - p(i_{n-1} - i_c)| \tag{20}$$

2.4 Feature fusion and classification

Following global feature extraction from the segmented masses, and local feature extraction from a ribbon of pixels surrounding the mass boundary, fusion of the two family of features is performed. To this end, feature normalization is performed on individual feature set followed by feature fusion. To exploit the correlation between the global and local features, principal component analysis (PCA) is performed on the feature vector obtained by concatenating global and local features. Various classifier models that include support vector machine (SVM), random forest (RF), multilayer perceptron (MLP) and extreme grading boosting classifier (XG Boost) are explored for differentiating benign and malignant masses [20-22]. As an implicit part of training, the hyperparameters of each of the models developed are tuned in the validation phase and the optimized models are employed for testing.

3. Results and Discussion

In this work, mammographic ROIs that include benign and malignant masses from the benchmark DDSM database are considered [23]. A total of 308 ROIs constituting 160 benign and 148 malignant tissue cases are used in the experiments.

Automated detection of masses is performed for global analysis using region growing process in which the seed points and thresholds are generated using GWO optimization. The threshold values obtained are in the range 0.08-0.012 across the different images considered. For local analysis, the ribbon of pixels along the boundary is extracted by employing dilation and erosion operations with a disc structuring element of radius 35, determined empirically. The fused global-local feature descriptor is used to train various classifier models. For comparative analysis, other experiments have also been performed, involving various feature extraction schemes. Specifically, the performance of models based on individual global and local analysis of the segmented ROI (schemes S_1 and S_2, respectively) is depicted in Table 3.1 and Table 3.2. Further, the results for local analysis on the ribbon of pixels surrounding the mass boundary (scheme S_3) is shown in Table 3.3.

It can be inferred from Table 3.1 that S_1 achieved a maximum accuracy of 80.6% with GLCM using RF and XG Boost classifier. Table 3.2 shows that S_2 achieved a maximum accuracy of 72.04% with SVM. Table 3.3 shows that the maximum accuracy for S_3 is 77.42% with RF.

Table 3.1 Comparison of various classifier models for S_1

Feature	Accuracy (%)			
	SVM	**RF**	**MLP**	**XG Boost**
GLCM	78.49	80.6	74.19	80.6
Morphology	67.74	44.08	59.13	50.53

Table 3.2 Comparison of various classifier models for S_2

Feature	Accuracy (%)			
	SVM	**RF**	**MLP**	**XG Boost**
LBP	72.04	68.8	62.3	66.6
SIFT	62.3	55.9	45.16	55.9

Table 3.3 Comparison of various classifier models for S_3

Feature	Accuracy (%)			
	SVM	RF	MLP	XG Boost
LBP	75.2	77.42	45.16	76.34
SIFT	62.3	58.06	45.16	64.52

Table 3.4 shows the results of the integrated descriptor analysis of the segmented ROI, wherein local features and global features are extracted from the ROI (scheme S_4). Table 3.5 depicts results of the proposed approach, which involves integration of global feature extracted from segmented ROI and local feature extracted from ribbon of pixels along mass boundary (scheme S_5). It can be inferred that the proposed approach (S_5) performs better as is evident from Table 3.4 and Table 3.5, yielding a maximum accuracy of 94.62% using a combination of morphological descriptors and GLCM (global) with SIFT (local) using multilayer perceptron (MLP) classifier.

Table 3.4 Comparison of various classifier models for S_4

Feature	Accuracy (%)			
	SVM	RF	MLP	XG Boost
Morphology-GLCM-SIFT	92.47	92.47	92.47	88.17
Morphology-GLCM-LBP	92.47	90.32	88.17	88.17

Table 3.5 Comparison of various classifier models for S_5 (Proposed approach)

Feature	Accuracy (%)			
	SVM	RF	MLP	XG Boost
Morphology-GLCM-SIFT	93.45	93.45	**94.62**	90.32
Morphology - GLCM-LBP	91.39	93.54	91.39	90.32

Comparative analysis of the best models across various feature extraction schemes is depicted in Fig. 3.1

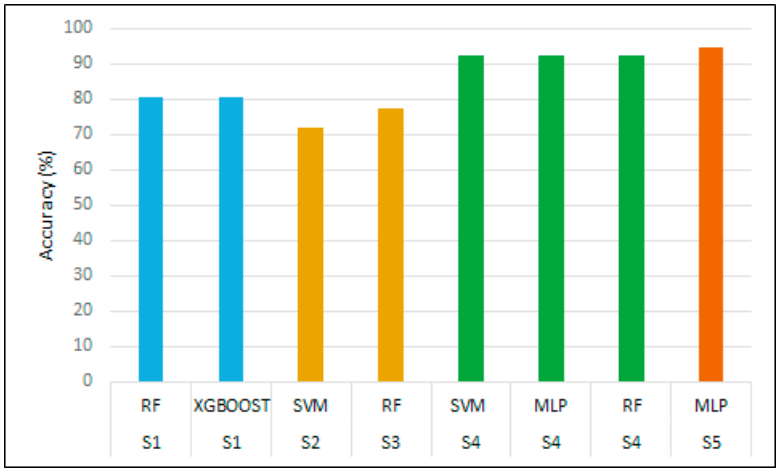

Fig. 3.1 Comparison of various feature extraction schemes

The confusion matrices of the two integrated feature analysis approaches, i.e., S_4 and S_5 are shown in Table 3.6 and Table 3.7. It can be observed from the tables that the proposed scheme S_5 achieves a reduction in both false positive rate (FPR) and false negative rate (FNR). The FPR and FNR of the proposed scheme are 4.8% and 5.7%, when compared to 9.3% and 6% respectively, for S_4.

Table 3.6 Confusion matrix: S_4

		Features			
		Morphology-GLCM-SIFT		Morphology-GLCM-LBP	
Classifier	**Class**	**Benign**	**Malignant**	**Benign**	**Malignant**
SVM	Benign	50	1	51	0
	Malignant	6	36	7	35
RF	Benign	47	4	48	3
	Malignant	3	39	6	36
MLP	Benign	47	4	44	7
	Malignant	3	39	4	38
XG Boost	Benign	45	6	46	5
	Malignant	5	37	6	36

Table 3.7 Confusion matrix: S_5 (Proposed approach)

		Features			
		Morphology-GLCM-SIFT		Morphology-GLCM-LBP	
Classifier	**Class**	**Benign**	**Malignant**	**Benign**	**Malignant**
SVM	Benign	51	0	50	1
	Malignant	6	36	7	35
RF	Benign	50	1	50	1
	Malignant	5	37	5	37
MLP	Benign	49	2	47	4
	Malignant	3	39	4	38
XG Boost	Benign	47	4	48	3
	Malignant	5	37	6	36

Table 3.8 Performance comparison with existing work

Reference	**Region of analysis**	**Feature extraction method**	**Accuracy (%) / AUC**
Midya et al. [8]	Ribbon of Pixels	Global (ACM)	81.23
Rabidas et al. [11]	Full ROI	Local (LPA)	80.76
El-Soud et al. [12]	Full ROI	Global + Local (OMI)	0.86
Integrated approach using full ROI based global and local analysis	Full ROI	Global (Morphology, GLCM) + Local (SIFT)	92.47
Proposed scheme	Full ROI + Ribbon of Pixels	Global - Full ROI (Morphology, GLCM) + Local - Ribbon of Pixels (SIFT)	94.6

Table 3.8 compares the performance of the proposed framework with state-of-the-art systems for mass characterization. For fair comparison, the table includes only results based on the work validated with DDSM database. The existing work have employed a broad range of methods that include global analysis on ribbon of pixels surrounding the mass boundary, local analysis on full ROI as well as combined global and local analysis on segmented ROI. Experimental results of the present work are also reproduced in Table 3.8. It can be observed that the proposed approach yields the highest performance, demonstrating its effectiveness in capturing comprehensive as well as minute details from mammograms for improved mass characterization.

4. Conclusion

The proposed work aims in developing a computer aided diagnosis (CAD) system for mass characterization using an integrated approach that combines global and local analysis. The system employs grey wolf optimization (GWO) based region growing algorithm for segmentation of regions of interest (ROI) followed by feature extraction. Global features including morphological features (shape and margin) and GLCM based texture features are extracted from segmented ROIs. In addition, SIFT based local features are also extracted from the ribbon of pixels surrounding the mass boundary. The resulting features are fused using principal component analysis (PCA). Multilayer perceptron model trained with the fused descriptor integrating the global and local features has yielded an accuracy as high as 94.62%, for classifying mammographic masses as benign or malignant. The proposed approach has achieved an improved performance when compared to state-of-the-art approaches for mass characterization.

References

[1] Bray, F., & Soerjomataram, I. (2015). The changing global burden of cancer: transitions in human development and implications for cancer prevention and control. *Cancer: disease control priorities*, *3*, 23-44. https://doi.org/10.1596/978-1-4648-0349-9_ch2

[2] Tang, J., Rangayyan, R. M., Xu, J., El Naqa, I., Yang, Y (2009) Computer-aided detection and diagnosis of breast cancer with mammography: recent advances. *IEEE Trans*. Inf. Technol. *Biomed.* 13(2):236-251. https://doi.org/10.1109/TITB.2008.2009441

[3] Verma, B., McLeod, P., Klevansky, A (2009) A novel soft cluster neural network for the classification of suspicious areas in digital mammograms. Pattern Recognit., 42(9):1845-1852. https://doi.org/10.1016/j.patcog.2009.02.009

[4] Liu, X., Tang, J (2013) Mass classification in mammograms using selected geometry and texture features, and a new SVM-based feature selection method. IEEE Syst. J. 8(3):910-920. https://doi.org/10.1109/JSYST.2013.2286539

[5] Wang, Y., Li, J., Gao, X (2014) Latent feature mining of spatial and marginal characteristics for mammographic mass classification. Neurocomputing, 144:107-118. https://doi.org/10.1016/j.neucom.2013.11.050

[6] Rouhi, R., Jafari, M., Kasaei, S., Keshavarzian, P (2015) Benign and malignant breast tumors classification based on region growing and CNN segmentation. Expert Syst. Appl. 42(3):990-1002. https://doi.org/10.1016/j.eswa.2014.09.020

[7] Mudigonda, Naga R., R. Rangayyan, JE Leo Desautels (2000) Gradient and texture analysis for the classification of mammographic masses. IEEE Trans. Med. Imaging 19(10):1032-1043. https://doi.org/10.1109/42.887618

[8] Midya, Abhishek, Jayasree Chakraborty (2015) Classification of benign and malignant masses in mammograms using multi-resolution analysis of oriented patterns. Proc. IEEE 12 Int. Symp. Biomed. Imaging. https://doi.org/10.1109/ISBI.2015.7163899

[9] Muramatsu, C., Hara, T., Endo, T., Fujita, H (2016) Breast mass classification on mammograms using radial local ternary patterns. Comput. Biol. Med. 72:43-53. https://doi.org/10.1016/j.compbiomed.2016.03.007

[10] Li, H., Zhuang, S., Li, D. A., Zhao, J., Ma, Y (2019) Benign and malignant classification of mammogram images based on deep learning. Biomed. Signal Process. Control 51:347-354. https://doi.org/10.1016/j.bspc.2019.02.017

[11] Rabidas, Rinku, Wasim Arif (2020) Characterization of mammographic masses based on local photometric attributes. Multimed. Tools. Appl. 79:21967-21985. https://doi.org/10.1007/s11042-020-08959-7

[12] El-Soud, M. W. A., Zyout, I., Hosny, K. M., Eltoukhy, M. M (2020) Fusion of Orthogonal Moment Features for Mammographic Mass Detection and Diagnosis. IEEE Access 8:129911-129923. https://doi.org/10.1109/ACCESS.2020.3008038

[13] Mirjalili, Seyedali, Seyed Mohammad Mirjalili, Andrew Lewis (2014) Grey wolf optimizer Adv. Eng. Softw. 69:46-61. https://doi.org/10.1016/j.advengsoft.2013.12.007

[14] Punitha, S., A. Amuthan, K. Suresh Joseph (2018) Benign and malignant breast cancer segmentation using optimized region growing technique Future Computing Inform. J. 3(2):348-358. https://doi.org/10.1016/j.fcij.2018.10.005

[15] Vadivel, A., B. Surendiran (2013) A fuzzy rule-based approach for characterization of mammogram masses into BI-RADS shape categories. Comput. Biol. Med. 43(4):259-267. https://doi.org 10.1016/j.compbiomed.2013.01.004

[16] Haralick, R. M., Shanmugam, K., Dinstein, I. H (1973) Textural features for image classification. IEEE Trans. Syst., Man, Cybern. (6):610-621. https://doi.org/10.1109/TSMC.1973.4309314

[17] Lowe, D. G (2004) Distinctive image features from scale-invariant keypoints. Int. J. Comput. Vis. 60(2):91-110. https://doi.org/10.1023/B:VISI.0000029664.99615.94

[18] Karthika, R., Latha Parameswaran (2018) An automated vision-based algorithm for out of context detection in images. Int. J. Signal Imaging Syst. Eng.11(1): 1-8. https://doi.org/10.1504/IJSISE.2018.090601

[19] Ojala, T., Pietikainen, M., Maenpaa, T (2002) Multiresolution gray-scale and rotation invariant texture classification with local binary patterns. IEEE Trans. Pattern Anal. Mach. Intell. 24(7):971-987. https://doi.org/10.1109/TPAMI.2002.1017623

[20] Vijayan, Devi, R. Lavanya (2021) Ensemble of density-specific experts for mass characterization in mammograms. Signal Image Video Process. 1-9. https://doi.org/10.1007/s11760-020-01826-w

[21] Balachandran, Dhadma, R. Lavanya (2016) Mass characterization in mammograms using an optimal ensemble classifier. IEEE Reg. 10 Annu. Int. Conf. Proc./TENCON: 2567-2570. https://doi.org/ 10.1109/TENCON.2016.7848500

[22] Toth, E., Kumar, S.S., Chaitanya, G., Riley, K., Balasubramanian, K, Pati, S (2020) Machine learning approach to detect focal-onset seizures in the human anterior nucleus of the thalamus. J. Neural Eng. 17(6):066004. https://doi.org/10.1088/1741-2552/abc1b7

[23] Heath, M., Bowyer, K., Kopans, D., Kegelmeyer, P., Moore, R., Chang, K., Munishkumaran, S (1998) Current status of the digital database for screening mammography. In Digital mammography Springer, Dordrecht:457-460. https://doi.org/10.1007/978-94-011-5318-8_75